PHYSICAL REVIEW B **86**, 020202(R) (2012)

Crystallization kinetics of nanocrystalline alloys revealed by *in situ* nuclear forward scattering of synchrotron radiation

M. Miglierini,[1,2,*] V. Prochazka,[2] S. Stankov,[3,4] P. Svec, Sr.,[5] M. Zajac,[6] J. Kohout,[7] A. Lancok,[8] D. Janickovic,[5] and P. Svec[5]

[1]*Institute of Nuclear and Physical Engineering, Slovak University of Technology, 812 19 Bratislava, Slovakia*

[2]*Regional Centre of Advanced Technologies and Materials, Palacky University, 771 46 Olomouc, Czech Republic*

[3]*Institute for Synchrotron Radiation, Karlsruhe Institute of Technology, Campus Nord, 76344 Eggenstein-Leopoldshafen, Germany*

[4]*Laboratory for Applications of Synchrotron Radiation, Karlsruhe Institute of Technology, Campus South, 76131 Karlsruhe, Germany*

[5]*Institute of Physics, Slovak Academy of Sciences, 845 11 Bratislava, Slovakia*

[6]*European Synchrotron Radiation Facility, BP 220, 38043 Grenoble, France*

[7]*Faculty of Mathematics and Physics, Charles University, 180 00 Prague, Czech Republic*

[8]*Institute of Inorganic Chemistry of the AS CR, v.v.i., 250 68 Husinec-Řež, Czech Republic*

(Received 30 August 2011; revised manuscript received 4 June 2012; published 31 July 2012)

The nanocrystallization kinetics of $Fe_{90}Zr_7B_3$ is investigated by *in situ* nuclear forward scattering of synchrotron radiation upon isothermal annealing. The nucleation and growth processes are accessed separately for the nanograins, their interfaces, and the residual amorphous matrix by monitoring the time evolution of the corresponding hyperfine parameters. This approach discloses the structural transformations taking place in this class of technologically important materials.

DOI: 10.1103/PhysRevB.86.020202 PACS number(s): 75.50.Tt, 61.46.Hk, 64.70.dg, 71.70.Jp

A central problem in nanotechnology is the understanding of the structure-to-properties relationship of the nanocrystalline interfaces that is essential for tailoring the functionalities, efficiency, and performance of near-future nanodevices consisting of subnanometer sized layers of material. The investigation of such buried layers, however, is a demanding experimental task. Direct methods used for imaging the interfaces, such as cross-sectional transmission electron microscopy, are destructive and do not allow for the observation of the structural changes that are taking place during nanograin growth and the formation of the interfaces. On the other hand, the information obtained by *in situ* techniques used for the investigation of the nanocrystallization kinetics is either averaged over the entire sample (differential scanning calorimetry) or over the distribution of electron densities (x-ray diffraction) and does not provide site-specific information.

The use of local probe techniques such as Mössbauer spectroscopy has offered unique opportunities to access the magnetic properties of the interfaces and nanograins separately.[1,2] Exploiting the fact that the hyperfine interactions instantly reflect the structural arrangement of the probe ^{57}Fe atom, it became possible to investigate the structural modifications of the sample by examining the hyperfine parameters that correspond to the Fe atoms located inside the nanograins, at their surfaces, or forming the interfaces.[3] Changes in microstructure, crystallization behavior, and the magnetic states of nanocrystalline alloys suggested that the interface regions play a significant role in the propagation of ferromagnetic exchange interactions between the nanograins through the amorphous matrix.[2,4–6] The relatively long acquisition times of a conventional Mössbauer spectrum (up to several hours), however, limited the application of this technique only to samples in equilibrium conditions having a well-defined crystallization state and prohibited the monitoring of the crystallization process itself.

Nanocrystalline alloys prepared by a controlled heat treatment of metallic glasses exhibit unique magnetic properties[7] that are caused by the size, amount, and chemical composition of the nanocrystallites embedded in a residual amorphous matrix.[8] Structural changes, related to crystallization, that occur in these materials, once exposed to elevated temperatures for prolonged operational times (sensors, transformer cores, recording devices, magnetic shielding, etc.[9]), deteriorate their performance. Therefore, a comprehensive understanding of the evolution of nanograins, interfaces, and the amorphous matrix during nanocrystallization is essential in order to understand, optimize, and conserve the unique magnetic properties exhibited by the nanocrystalline alloys. Among this class of materials the pioneering $Fe_{90}Zr_7B_3$ Nanoperm[10] still attracts considerable attention and was established as a model system for studying the structural,[11] dynamic,[12,13] and magnetic[14] properties of ternary nanocrystalline alloys.

In this Rapid Communication we report on the investigation of the nanocrystallization kinetics in $Fe_{90}Zr_7B_3$ separately for the nanograins, interface layers, and residual amorphous matrix by nuclear forward scattering of synchrotron radiation. The outstanding brilliance of the x-ray beams produced by third generation synchrotrons ensures rapid recording of time spectra, allowing for a direct *in situ* observation of dynamical processes that are taking place during heat treatment. Employing the fact that hyperfine interactions instantly reflect the state of the structural arrangement by examination of the corresponding hyperfine parameters during nanocrystallization, it is now possible to follow separately the structural evolution of different sites of the ^{57}Fe probe atoms. The obtained results are used to thoroughly assess the available models for nucleation and nanograin growth upon an isothermal annealing of this class of technologically important materials.

A $Fe_{90}Zr_7B_3$ amorphous alloy enriched to 63% in ^{57}Fe was prepared by a melt-spinning technique in a form of 2 mm wide and 20 μm thick ribbons. The as-quenched alloy contained bcc Fe nanocrystals that were identified in the surface regions of the ribbon by conversion electron Mössbauer spectrometry.[13] As

 ©2012 American Physical Society

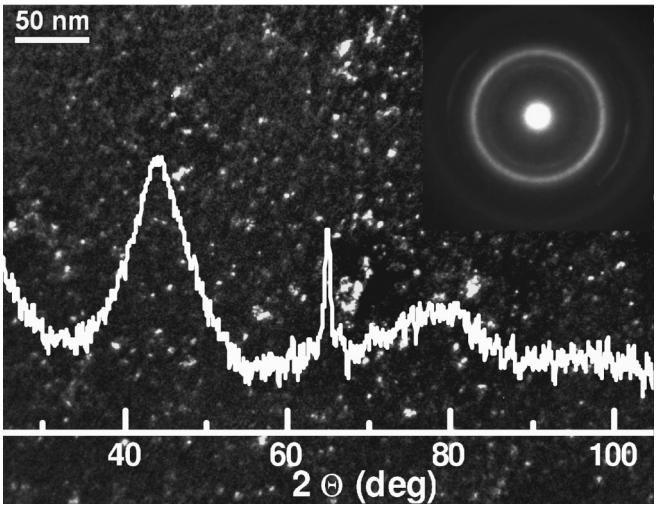

FIG. 1. Transmission electron micrograph (dark field) of the as-quenched $Fe_{90}Zr_7B_3$ alloy. Electron and x-ray diffraction patterns are also included.

demonstrated in Fig. 1, they were found also in the bulk of the ribbon, amounting to approximately 2.5% with sizes of about 2 nm determined by x-ray diffraction, electron diffraction, and transmission electron microscopy. The narrow [002] reflection at 65° indicates a strong preferential orientation of the quenched-in nanocrystals, which is confirmed also by an intensity variation of some electron diffraction rings. In addition, a Zr content of about 0.2% was identified inside the bcc Fe nanograins.[14] Nuclear forward scattering experiments were carried out at the Nuclear Resonance end station ID22N of the European Synchrotron Radiation Facility. We used photons with an energy of 14.413 keV and an energy resolution of about 3 meV. The sample was placed inside a vacuum furnace and heated up to a temperature of 743 K with a ramp of 40 K/min. An isothermal experiment at this temperature was performed for up to 130 min. The temperature of the experiment was chosen close to the onset of crystallization at 783 K determined from differential scanning calorimetry.[13] The time spectra of nuclear forward scattering were continuously recorded with an acquisition time of 1 min.

A contour plot obtained from a three-dimensional (3D) image of all 130 spectra is illustrated in Fig. 2(a). The elapsed decay time of the nuclear resonant level and the time of annealing are displayed on the x and y axes, respectively. The measured intensities are color coded in a logarithmic scale. Selected time spectra obtained after annealing for 15, 40, and 120 min are shown in Fig. 2(b). All spectra were consistently analyzed with the CONUSS code.[15] The amorphous matrix was reconstructed by a distribution of electric quadrupole interactions (quadrupole splitting) corresponding to its paramagnetic state above the Curie point at a given temperature. The nanocrystalline phase of bcc Fe formed upon annealing was associated with a spectral component featuring magnetic dipole interactions with a unique value of the hyperfine magnetic field [open circles in Fig. 3(a)]. The third component is ascribed to iron atoms that are localized at the surfaces of nanocrystalline grains buried inside the amorphous phase. These atoms exhibit symmetry different from those in the nanograins. They belong to the interface regions and were refined from the spectra using a distribution of magnetic hyperfine fields with average values plotted as open triangles in Fig. 3(a). The presence of this spectral component was revealed by conventional Mössbauer effect experiments[1,2,16,17] performed under static conditions.

The relative contents of amorphous, nanograin, and interface components, isomer shifts of the amorphous and interface fractions determined relative to that of the nanocrystalline phase, quadrupole splitting of the amorphous and interface fractions, hyperfine magnetic fields of the nanograins and interfaces, as well as the Debye temperature, an intensity scaling factor, and shift along the time scale were free

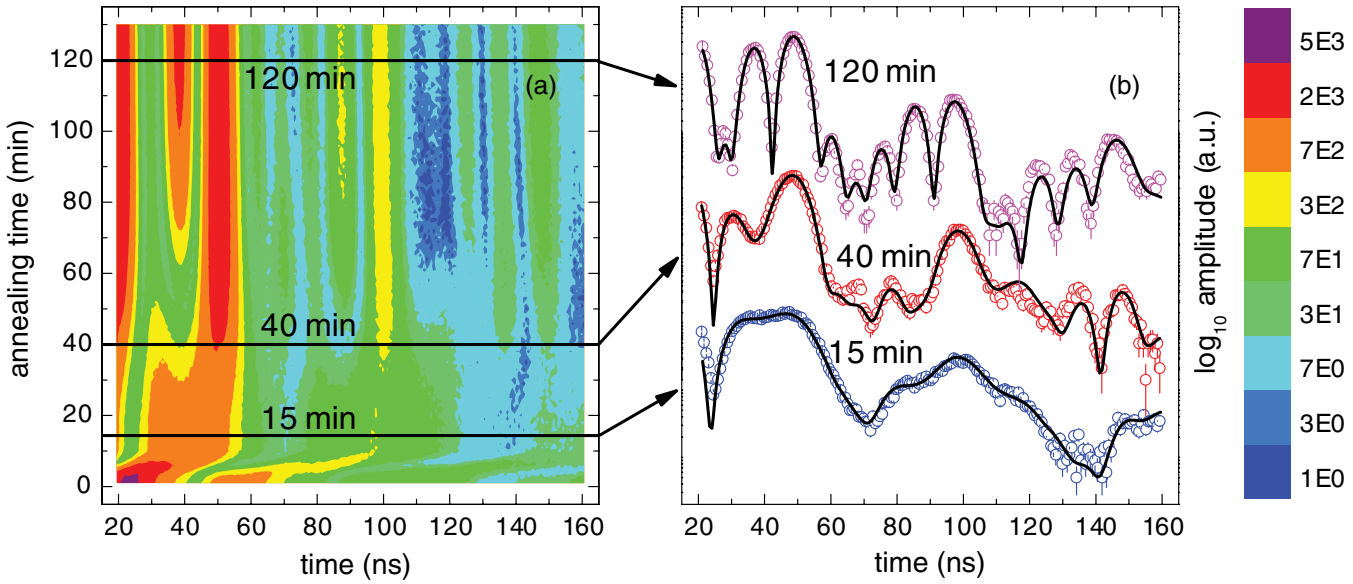

FIG. 2. (Color online) Contour plot of 3D nuclear forward scattering spectra of $Fe_{90}Zr_7B_3$ annealed at 743 K (a) and selected records (open symbols) with fits (solid lines) for 15, 40, and 120 min of annealing (b).

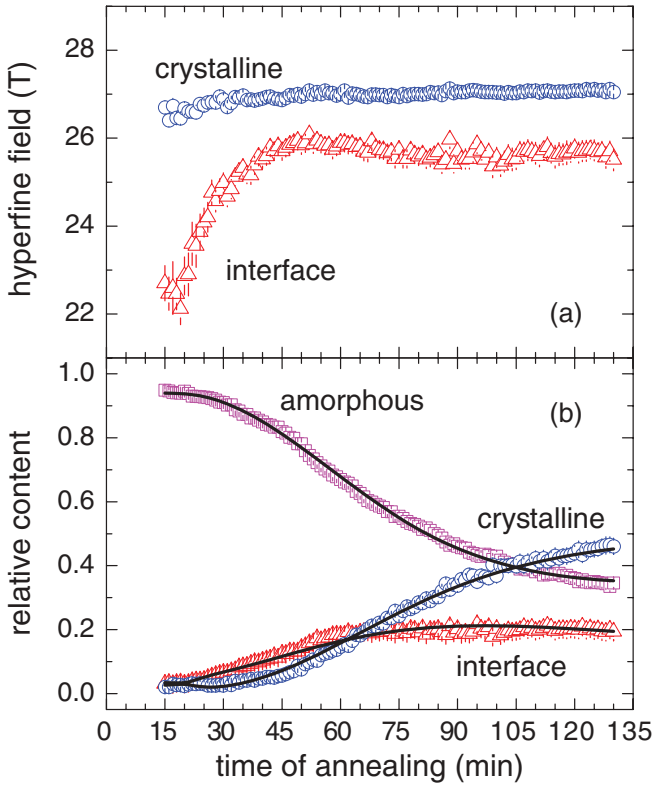

FIG. 3. (Color online) Time evolution of the hyperfine magnetic fields (a) and relative content of spectral components (b) derived from the analysis of nuclear forward scattering spectra recorded at 743 K (open symbols). Solid lines in (b) represent fits between theoretically calculated (according to the model described in the text) and experimentally obtained data.

parameters during analysis. The quadrupole splitting and isomer shift of the nanograin component were set to zero and fixed.

The time dependencies of hyperfine fields and relative fractions of the components derived from the consistent analysis of the time spectra from Fig. 2 are shown in Figs. 3(a) and 3(b), respectively. After reaching the temperature of isothermal annealing at the 15th minute, the relative contents are almost constant for about 5 min up to the 20th minute of annealing. The values of the hyperfine magnetic fields at 743 K are reduced due to superparamagnetic behavior at this elevated temperature. Within the following 15 min (up to the 35th min) new grains with subnanometer sizes are formed around the existing nucleation centers. This is revealed by an increase of interfacial regions (when nearly all atoms constitute predominantly the nanograin surface) while the amount of Fe atoms located inside the nanograins remains unaffected [Fig. 3(b)]. The enhanced contribution of the interfaces is also indirectly confirmed by a significant increase of the corresponding values of the hyperfine field, as depicted in Fig. 3(a). Simultaneously the amount of iron located inside the amorphous residual matrix gradually diminishes.

The nanograin content steadily rises after about 40 min of heat treatment, together with the interface component, while the depletion of Fe in the residual material continues. At this moment the growing nanograins reach their size and density that correspond to the final values of the hyperfine fields for the nanograins and interfaces [Fig. 3(a)]. After about 60 min of annealing the relative fraction of interfaces seemingly saturates and only the nanograin fraction continues to rise on account of the residual amorphous matrix. This behavior clearly indicates a nanograin growth process. The amount of Fe in the bulk of nanocrystals increases more rapidly compared to that at their surfaces. The increased number and density of nanograins eventually leads to the formation of agglomerates which effectively suppresses the contribution of the interface fraction while the number of Fe atoms positioned within the nanograins rises. At this stage, the average grain size reached a final value of 12 ± 3 nm, as derived from x-ray diffraction patterns.[12]

The hyperfine field corresponding to the nanograins coincides with the value reported from Mössbauer effect experiments for bcc Fe at a particular temperature of the experiment.[18] The interfaces are characterized with systematically lower (by 1–2 T) values of the hyperfine fields when their relative content is stabilized. This is in agreement with the results from high-temperature Mössbauer effect experiments performed upon the same nanocrystalline alloy.[6] The relative atomic fraction of the interface component increases only up to a certain value determined by the size and the amount of the nanograins. The hyperfine fields of the interfaces are low at the onset of crystallization due to a significant influence of the surrounding paramagnetic amorphous matrix, and they reach their final values when the first and second coordinations of iron atoms are completed and stabilized. The values of the hyperfine fields are also governed by the broken translational symmetry experienced by the ^{57}Fe atoms positioned at the surface of the nanograins. From one side they are surrounded by the perfect long-range ordered atoms of the nanograin interior. The amorphous matrix, which is positioned from the other side of the interface atoms, implies lower values of the hyperfine fields because it contains an effectively higher concentration of nonmagnetic elements. They are accumulated namely in close proximity to the newly developed Fe nanograins, as demonstrated by atom probe field ion microscopy,[19] which might further contribute to the observed decrease of the magnetic fields. This effect is more pronounced than a possible contribution of nonmagnetic atoms positioned in the nanocrystalline lattice itself, which was estimated to be about 0.2% Zr.[14]

The unique possibility to investigate the time evolution of the nanograins, interfaces, and the residual amorphous matrix separately upon isothermal annealing allowed for assessing the crystallization kinetics in this nanocrystalline alloy. We have considered crystallization according to the Johnson-Mehl-Avrami nucleation (site saturation nucleation), grain growth, and impingement[20] extended by a simplified model that assumes two types of spherelike grains: quenched-in grains (Q) and newly formed grains (F). We have assumed that the grains consist of a surface layer and a core. The thickness of the former was kept constant with annealing time during simulation. The experimentally obtained time dependencies of the spectral components [symbols in Fig. 3(b)] were reproduced by taking into account the contributions from the surface layers and the bulk of the grains.[20] The time evolution of the relative weights of the amorphous residual

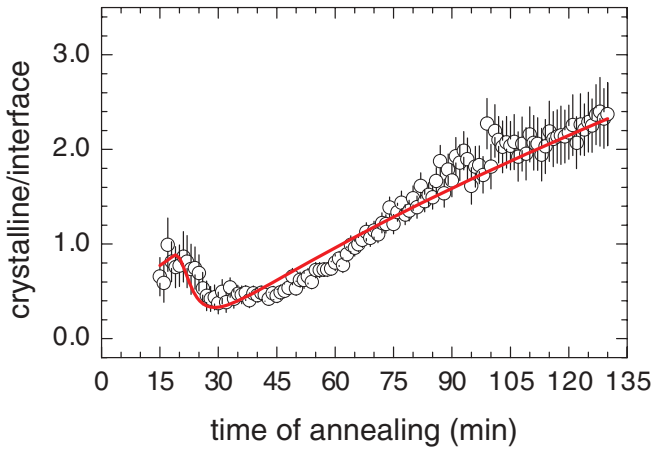

FIG. 4. (Color online) Ratio of the relative contents of crystalline and interface components as a function of annealing time at 743 K: Open symbols, experimental data; solid line, ratio of fits from theoretical calculations.

matrix (W_{AM}), interface regions (W_{IF}), and nanocrystals (W_{NC}) are expressed as

$$W_{AM} = (1 - C_0) + (C_0 - C_\infty) \cdot \left[1 - \exp\left(-\frac{4}{3}\pi \int_0^{t-t_0} N(\tau) \cdot [(t-\tau) \cdot v]^w d\tau\right)\right], \quad (1)$$

where τ is the time for formation of $N(\tau)d\tau$ new grains which grow with speed v, w describes the grain growth process, C_0 and C_∞ represent the amount of phase before and after the transformation, respectively,

$$W_{IF} = (1 - W_{AM})\frac{RQ_{IF} + (1-R)F_{IF}}{Q + F}, \quad (2)$$

$$W_{NC} = (1 - W_{AM})\frac{RQ_{NC} + (1-R)F_{NC}}{Q + F}, \quad (3)$$

with Q and F being integral volumes of all quenched-in and newly formed grains at time t, respectively, subscripts IF and NC denote contributions from interfaces (surface layer) and interiors of the grains (core), and R stands for the ratio of the number of quenched-in and newly formed grains.

This model assumes that all nucleation centers are formed at the beginning of the crystallization and that the rate of grain growth is governed by the Avrami exponent $n = 2.0 \pm 0.2$. Using Eqs. (1)–(3), the time dependencies of the relative contents of all three components were fitted to the experimentally obtained data. The solid curves in Fig. 3(b) represent the resulting fits. This figure reveals a very good agreement between the experimentally obtained and theoretically calculated data for all three components along the duration of the entire experiment.

In Fig. 4, the evolution of the experimentally obtained ratio of the relative contents of the crystalline and interface components (symbols) is plotted as a function of annealing time. It is superimposed with a solid line obtained from the fits from Fig. 3(b). It should be noted that in this representation all possible deviations between the experimental and theoretical time dependencies for crystalline and interface components that are hardly seen in Fig. 3(b) now become visible. This comparison reveals that the experimental results are fully consistent with the calculated time dependencies even for tiny details seen at an early stage of the annealing process.

The quenched-in nanocrystallites manifest themselves at the very beginning with a certain bulk-to-surface (i.e., crystalline/interface) ratio. After the 20th minute of annealing, new nanograins are formed. Their small dimensions favor a higher contribution of the interface component because the majority of atoms form the grain surfaces. This is indicated by a decrease of the crystalline/interface ratio. Finally, from about the 35th minute, the grain grow process starts and the ratio steadily increases due to a higher contribution of the bulk of the grains.

The deviations between the experimentally measured and theoretically calculated data which are seen between the 45th and the 65th minute of annealing arise most likely from the fact that in our model we have calculated the evolution of an individual grain without taking into account the presence of the neighboring grains. In reality, however, the growth of grains is constrained due to impingement. This means that the grain growth is limited when the grains approach each other or when they are in very close proximity to the neighboring grains and surrounded by an increased concentration of Zr and B atoms.[19,21] Consequently, the contribution of the surface layers shows a tendency to saturate whereas the bulk of the grains still rises. The interface layer thickness towards the end of annealing is about 0.7 nm, which is in agreement with 0.6 nm reported in Ref. 1.

In conclusion, by applying nuclear forward scattering of synchrotron radiation *in situ* in the course of isothermal heating of $Fe_{90}Zr_7B_3$ Nanoperm, we were able to follow the time evolution of hyperfine interactions for the nanograins, interfaces, and the residual amorphous matrix separately. The obtained results were employed to thoroughly assess the available models for nucleation and grain growth upon an isothermal annealing of the amorphous precursor to fine details.

Even though the overall formation of nanocrystals can be deduced also from other analytical techniques, the approach proposed here provides the possibility to study separately the contributions of Fe atoms positioned at different locations within the interior or at the surface of the nanograins comprising also their hyperfine interactions. Furthermore, applied at different annealing temperatures and to alloys with various compositions, this method can provide information about the crystallization kinetics of the technologically important family of nanocrystalline materials prepared by controlled crystallization of an amorphous precursor.

This work was supported by Grants No. VEGA 1/0286/12, No. APVV-0492-11, No. MSM0021620834, and No. P204/10/0035, and by the Operational Program Research and Development for Innovations European Regional Development Fund (CZ.1.05/2.1.00/03.0058) and the Operational Program Education for Competitiveness European Social Fund (Project No. CZ.1.07/2.3.00/20.0017). S.S. acknowledges support by the Helmholtz Association (VH-NG-625).

*marcel.miglierini@stuba.sk

[1]A. Slawska-Waniewska and J. M. Greneche, Phys. Rev. B **56**, 8491 (1997).
[2]M. Miglierini and J. M. Greneche, J. Phys.: Condens. Matter **9**, 2321 (1997).
[3]M. Miglierini and J. M. Greneche, J. Phys.: Condens. Matter **9**, 2303 (1997).
[4]K. Suzuki and J. M. Cadogan, Phys. Rev. B **58**, 2730 (1998).
[5]J. M. Greneche, N. Randrianantoandro, A. Slawska-Waniewska, and M. Miglierini, Hyperfine Interact. **113**, 279 (1998).
[6]S. Stankov, B. Sepiol, T. Kanuch, D. Scherjau, R. Würschum, and M. Miglierini, J. Phys.: Condens. Matter **17**, 3183 (2005).
[7]K. Suzuki, A. Makino, A. Inoue, and T. Masumoto, J. Appl. Phys. **70**, 6232 (1991).
[8]G. Herzer, Phys. Scr., T **49A**, 307 (1993).
[9]M. E. McHenry and D. E. Laughlin, Acta Mater. **48**, 223 (2000).
[10]K. Suzuki, N. Kataoka, A. Inoue, A. Makino, and T. Masumoto, Mater. Trans., JIM **31**, 743 (1990).
[11]T. Ohkubo, H. Kai, A. Makino, and Y. Hirotsu, Mater. Sci. Eng., A **312**, 274 (2001).
[12]S. Stankov, Y. Z. Yue, M. Miglierini, B. Sepiol, I. Sergueev, A. I. Chumakov, L. Hu, P. Svec, and R. Rüffer, Phys. Rev. Lett. **100**, 235503 (2008).
[13]S. Stankov, M. Miglierini, A. I. Chumakov, I. Sergueev, Y. Z. Yue, B. Sepiol, P. Svec, L. Hu, and R. Rüffer, Phys. Rev. B **82**, 144301 (2010).
[14]M. Miglierini, A. Lancok, and J. Kohout, Appl. Phys. Lett. **96**, 211902 (2010).
[15]W. Sturhahn and E. Gerdau, Phys. Rev. B **49**, 9285 (1994).
[16]T. Kemény, D. Kaptás, J. Balogh, L. F. Kiss, T. Pusztai, and I. Vincze, J. Phys.: Condens. Matter **11**, 2841 (1999).
[17]J. Balogh, L. Bujdosó, D. Kaptás, T. Kemény, I. Vincze, S. Szabó, and D. L. Beke, Phys. Rev. B **61**, 4109 (2000).
[18]R. S. Preston, S. S. Hanna, and J. Heberle, Phys. Rev. **168**, 2207 (1962).
[19]K. Hono, Y. Zhang, A. Inoue, and T. Sakurai, Mater. Sci. Eng., A **226–228**, 498 (1997).
[20]F. Liu, F. Sommer, and E. J. Mittemeijer, J. Mater. Sci. **39**, 1621 (2004).
[21]E. Pineda and D. Crespo, Phys. Rev. B **60**, 3104 (1999).